

# Meson-Hybrid Mixing in Vector ( $1^{--}$ ) and Axial Vector ( $1^{++}$ ) Charmonium

D. Harnett

*Department of Physics, University of the Fraser Valley, Abbotsford, BC, Canada, V2R 3E7*

A. Palameta, J. Ho, and T. G. Steele

*Department of Physics and Engineering Physics,  
University of Saskatchewan, Saskatoon, SK, Canada, S7N 5E2*

We study mixing between conventional and hybrid mesons in vector and axial vector charmonium using QCD Laplace sum-rules. We compute meson-hybrid cross correlators within the operator product expansion, taking into account condensate contributions up to and including those of dimension-six as well as composite operator renormalization-induced diagrams. Using measured masses of charmonium-like states as input, we probe known resonances for nonzero coupling to both conventional and hybrid meson currents, a signal for meson-hybrid mixing.

## I. INTRODUCTION

Hybrid mesons are hadrons containing a constituent quark, antiquark, and gluon. As they are colour singlets, they should be observable. Despite decades of searching, they have yet to be conclusively identified in experiment. Hadron mixing, the idea that observed hadrons might be superpositions of conventional (i.e., quark-antiquark) mesons, hybrid mesons, tetraquarks, etc. . . , could be hampering identification.

To explore this idea, we consider the XYZ resonances, a collection of charmonium-like states many of which are not readily interpreted as conventional mesons. (For a review, see [1].) We focus on the vector (i.e.,  $J^{PC} = 1^{--}$ ) and axial vector (i.e.,  $J^{PC} = 1^{++}$ ) channels. Known resonances in these channels are listed in Tables I and II [2].

TABLE I: Known charmonium-like vector (i.e.,  $J^{PC} = 1^{--}$ ) resonances.

Name	Mass (GeV)
$J/\psi$	3.10
$\psi(2S)$	3.69
$\psi(3770)$	3.77
$\psi(4040)$	4.04
$\psi(4160)$	4.19
$X(4230)$	4.23
$X(4260)$	4.23
$X(4360)$	4.34
$\psi(4415)$	4.42
$X(4660)$	4.64

We test the resonances of Tables I and II for coupling to a conventional meson-hybrid meson cross-correlator using QCD Laplace sum-rules (LSRs). QCD sum-rules are transformed dispersion relations that relate a QCD-computed correlator to an integral over a hadronic spectral function [3, 4]. Using measured resonance masses (and effective widths) as

TABLE II: Known charmonium-like axial vector (i.e.,  $J^{PC} = 1^{++}$ ) resonances.

Name	Mass (GeV)
$\chi_{c1}(1P)$	3.51
$X(3872)$	3.87
$X(4140)$	4.15
$X(4274)$	4.27

input, we extract products of conventional meson and hybrid meson couplings, i.e., mixing parameters, as best-fit parameters between QCD and hadron physics. Resonances with nonzero mixing parameters can be interpreted as having both conventional meson and hybrid meson components.

## II. CORRELATORS

Consider the charmonium-like conventional meson-hybrid meson cross-correlator,

$$\Pi(q^2) = \frac{i}{D-1} \left( \frac{q_\mu q_\nu}{q^2} - g_{\mu\nu} \right) \times \int d^D x e^{iq \cdot x} \langle \Omega | \tau j_\mu^{(m)}(x) j_\nu^{(h)}(0) | \Omega \rangle, \quad (1)$$

for spacetime dimension  $D$  between conventional meson current

$$j_\mu^{(m)} = \begin{cases} \bar{c} \gamma_\mu c & \text{for } 1^{--} \\ \bar{c} \gamma_\mu \gamma_5 c & \text{for } 1^{++} \end{cases} \quad (2)$$

and hybrid meson current

$$j_\nu^{(h)} = \begin{cases} g_s \bar{c} \gamma^\rho \gamma_5 \frac{\lambda^a}{2} \left( \frac{1}{2} \epsilon_{\nu\rho\omega\eta} G_{\omega\eta}^a \right) c & \text{for } 1^{--} \\ g_s \bar{c} \gamma^\rho \frac{\lambda^a}{2} \left( \frac{1}{2} \epsilon_{\nu\rho\omega\eta} G_{\omega\eta}^a \right) c & \text{for } 1^{++} \end{cases} \quad (3)$$

In (2) and (3),  $c$  is a charm quark,  $G_{\omega\eta}^a$  is the gluon field strength, and  $\epsilon_{\nu\rho\omega\eta}$  is the Levi-Civita symbol.

We compute  $\Pi(Q^2)$  using the operator product expansion (OPE) in which perturbation theory is supplemented by nonperturbative corrections, each of which is the product of a perturbatively computed Wilson coefficient and a nonzero vacuum expectation value, i.e., a condensate. We consider condensates of dimension-six (i.e., 6d) or less. Wilson coefficients are computed to leading-order in  $\alpha_s = \frac{g_s}{4\pi}$ . The diagrams that contribute are shown in Fig. 1. Computational details and correlator results can be found in [5, 6].

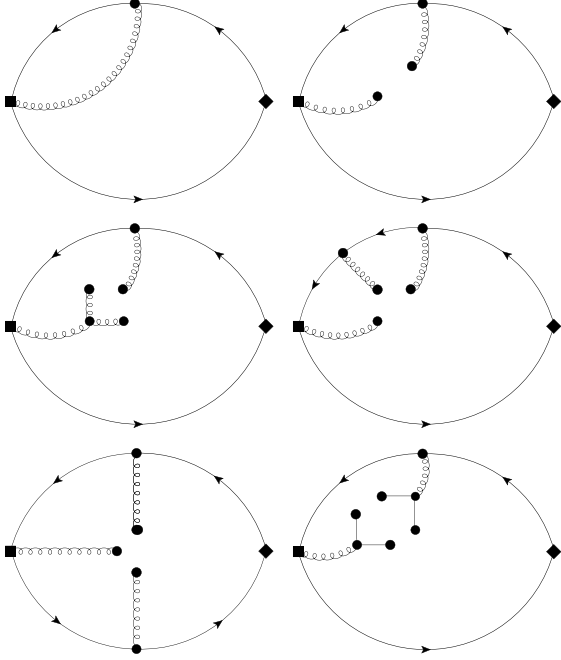


FIG. 1: The diagrams calculated for  $\Pi(Q^2)$  from (1). The diagram in the upper left is perturbation theory. The others are nonperturbative condensate contributions. Square vertices represent the hybrid meson current (3). Diamond vertices represent the conventional meson current (2). All Feynman diagrams in this manuscript were produced with JaxoDraw [7].

The perturbative contribution to  $\Pi(Q^2)$  contains a nonlocal divergence eliminated through operator mixing under renormalization of the hybrid meson current (3). The replacements,

$$j_\nu^{(h)} \rightarrow j_\nu^{(h)} - \frac{5g_s^2 m^2}{18\pi^2 \epsilon} \bar{c}\gamma_\nu c + \frac{g_s^2 m}{9\pi^2 \epsilon} \bar{c}iD_\nu c \text{ for } 1^{--},$$

$$j_\nu^{(h)} \rightarrow j_\nu^{(h)} - \frac{5g_s^2 m^2}{18\pi^2 \epsilon} \bar{c}\gamma_\nu \gamma_5 c - \frac{g_s^2 m}{9\pi^2 \epsilon} \bar{c}i\gamma_5 D_\nu c \text{ for } 1^{++},$$

for covariant derivative operator  $D_\nu$  lead to two renormalization-induced diagrams shown in Fig. 2. These two diagrams cancel the nonlocal divergence and provide nontrivial contributions to the finite part of perturbation theory. Again, computational details and results can be found in [5, 6].

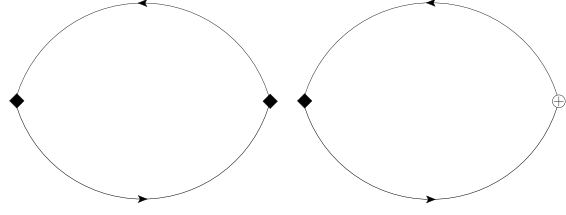


FIG. 2: The renormalization-induced diagrams that contribute to  $\Pi(Q^2)$  from (1). Diamond vertices represent the conventional meson current (2). Thus circle-plus vertex corresponds to the covariant derivative current  $\bar{c}iD_\nu c$  in the vector channel and  $\bar{c}i\gamma_5 D_\nu c$  in the axial vector channel.

### III. LAPLACE SUM-RULES

The function  $\Pi(Q^2)$  satisfies a dispersion relation,

$$\Pi(Q^2) = \frac{Q^6}{\pi} \int_{t_0}^{\infty} \frac{\text{Im}\Pi(t)}{t^3(t+Q^2)} dt + \dots, \quad (4)$$

for  $Q^2 = -q^2 > 0$  where  $t_0$  is a hadron production threshold. On the left-hand side,  $\Pi(Q^2)$  is identified with the correlator computed in Section II, denoted  $\Pi^{\text{QCD}}(Q^2)$  from here on. On the right-hand side, the hadronic spectral function,  $\text{Im}\Pi(t)$ , is decomposed as

$$\frac{1}{\pi} \text{Im}\Pi(t) = \rho^{\text{had}}(t) + \frac{1}{\pi} \text{Im}\Pi^{\text{QCD}}(t)\Theta(t-s_0) \quad (5)$$

where  $\Theta(t-s_0)$  is a Heaviside step function at continuum threshold  $s_0$  and  $\rho^{\text{had}}(t)$ , the resonance content, is modelled as

$$\rho^{\text{had}}(t) = \sum_{i=1}^n \xi_i \delta(t - m_i^2). \quad (6)$$

where  $m_i$  are resonance masses and  $\xi_i$  are mixing parameters. A resonance with nonzero mixing parameter couples to both conventional and hybrid meson currents. Specific resonance models are defined in Tables III and IV for the vector and axial vector channels respectively. Note that, in the vector channel, some densely packed resonances are amalgamated as resonances clusters. For these clusters, the corresponding  $\delta$ -function in (6) is replaced by a rectangular ‘‘pulse’’ to account for the nonzero width  $\Gamma$ .

Subtracted LSRs are defined as [3, 4]

$$\mathcal{R}^{\text{QCD}}(\tau, s_0) = \frac{1}{\tau} \lim_{\substack{N, Q^2 \rightarrow \infty \\ \tau = N/Q^2}} \frac{(-Q^2)^N}{\Gamma(N)} \left( \frac{d}{dQ^2} \right)^N \Pi^{\text{QCD}}(Q^2) - \int_{s_0}^{\infty} e^{-t\tau} \frac{1}{\pi} \text{Im}\Pi^{\text{QCD}}(t) dt \quad (7)$$

where  $\tau$  is the Borel parameter. Then, eqns. (4)–(7) imply that  $\mathcal{R}^{\text{QCD}}(\tau, s_0) = \mathcal{R}^{\text{had}}(\tau; \{\xi_i\})$  where [5, 6]

$$\mathcal{R}^{\text{had}}(\tau; \{\xi_i\}) = \int_0^{s_0} e^{-t\tau} \rho^{\text{had}}(t) dt. \quad (8)$$

TABLE III: A representative collection of hadron models analyzed in the vector sector.

Model	$m_1$ (GeV)	$\Gamma_1$ (GeV)	$m_2$ (GeV)	$\Gamma_2$ (GeV)	$m_3$ (GeV)	$\Gamma_3$ (GeV)
V1	3.10	0	-	-	-	-
V2	3.10	0	3.73	0	-	-
V3	3.10	0	3.73	0	4.30	0
V4	3.10	0	3.73	0	4.30	0.30
V5	3.10	0	3.73	0.05	4.30	0.30
V6	3.10	0	-	-	4.30	0
V7	3.10	0	-	-	4.30	0.30

TABLE IV: A representative collection of hadron models analyzed in the axial vector sector.

Model	$m_1$ (GeV)	$m_2$ (GeV)	$m_3$ (GeV)	$m_4$ (GeV)
A1	3.51	-	-	-
A2	3.51	3.87	-	-
A3	3.51	3.87	4.15	-
A4	3.51	3.87	4.15	4.27

#### IV. ANALYSIS AND RESULTS

For each of the hadron models of Tables III and IV, we extract mixing parameters  $\{\xi_i\}$  and a continuum threshold  $s_0$  as best-fit values between (7) and (8). To do so, we minimize the chi-square,

$$\chi^2(s_0; \{\xi_i\}) = \sum_{\tau_{\min}}^{\tau_{\max}} (\mathcal{R}^{\text{QCD}}(\tau, s_0) - \mathcal{R}^{\text{had}}(\tau; \{\xi_i\}))^2, \quad (9)$$

over a (discretized) interval of acceptable  $\tau$ -values ( $\tau_{\min}, \tau_{\max}$ ). (See [5, 6] for more detail.) Results are given in Table V and Table VI for the vector and axial vector models respectively. Instead of  $\xi_i$ , we present  $\zeta$  and  $\frac{\xi_i}{\zeta}$  where

$$\zeta = \sum_{i=1}^n |\xi_i| \quad (10)$$

and where  $n$  is the number of resonances in the model in question. Also, the given minimized values of (9) have been scaled by the minimized value for the single narrow resonance model in each channel, i.e., Model V1 in the vector channel and Model A1 in the axial vector channel. We plot relative residuals,

$$\frac{\mathcal{R}^{\text{QCD}}(\tau, s_0) - \mathcal{R}^{\text{had}}(\tau, \{\xi_i\})}{\mathcal{R}^{\text{QCD}}(\tau, s_0)}, \quad (11)$$

versus  $\tau$  in Fig. 3 for a representative set of vector models and in Fig. 4 and for a representative set of axial vector models.

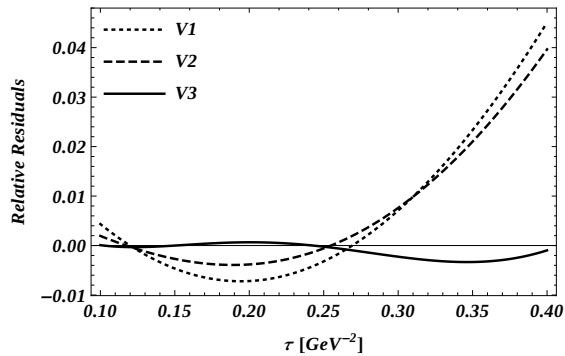
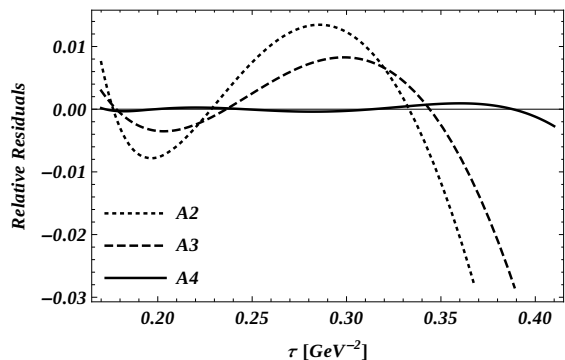

 FIG. 3: Relative residuals (11) versus Borel parameter  $\tau$  for a representative set of hadron models in the vector channel (i.e., from Table III).


FIG. 4: The same as Fig. 3 but for models in the axial vector channel (i.e., from Table IV).

#### V. DISCUSSION

From the normalized chi-squares in Tables V and VI, we see that agreement between theoretically calculated LSRs and hadron physics is significantly improved by including both excited resonances and the ground state in the hadron model. Based on chi-squares values and the relative residuals plotted in Figs. 3 and 4, we favour Models V3–V7 in the vector channel (all of which lead to essentially the same conclusions) and Model A4 in the axial vector channel. Note that the resonance widths in Models V4, V5, and V7 have little effect on the results. This is unsurprising as LSRs are generally insensitive to symmetric resonance widths. By design, LSRs exponentially suppress contributions from heavy resonances relative to lighter ones, and so it is important to check that the heavy resonances of Models V3–V7 and A4 make numerically significant contributions. As a quantitative measure in, for example, Model V3, consider

$$\frac{|\xi_3| \int_{\tau_{\min}}^{\tau_{\max}} e^{-m_3^2 \tau} d\tau}{\sum_{i=1}^3 |\xi_i| \int_{\tau_{\min}}^{\tau_{\max}} e^{-m_i^2 \tau} d\tau}, \quad (12)$$

TABLE V: Predicted mixing parameters with theoretical uncertainties and continuum thresholds for the vector hadron models of Table III.

Model	$s_0$ (GeV <sup>2</sup> )	$\frac{\chi^2}{\chi^2(V1)}$	$\zeta$ (GeV <sup>6</sup> )	$\frac{\xi_1}{\zeta}$	$\frac{\xi_2}{\zeta}$	$\frac{\xi_3}{\zeta}$
V1	12.5	1	0.51(2)	1	-	-
V2	13.9	0.73	0.73(4)	0.73(3)	0.27(3)	-
V3	24.1	0.038	2.9(3)	0.22(1)	-0.022(5)	0.76(3)
V4	24.2	0.037	3.0(3)	0.21(1)	-0.032(5)	0.76(3)
V5	24.2	0.037	3.0(3)	0.21(1)	-0.032(5)	0.76(3)
V6	23.7	0.042	2.7(2)	0.23(2)	-	0.77(2)
V7	23.6	0.047	2.7(2)	0.23(2)	-	0.77(2)

TABLE VI: The same as Table V but for the hadron models of Table IV.

Model	$s_0$ (GeV <sup>2</sup> )	$\frac{\chi^2}{\chi^2(V1)}$	$\zeta$ (GeV <sup>6</sup> )	$\frac{\xi_1}{\zeta}$	$\frac{\xi_2}{\zeta}$	$\frac{\xi_3}{\zeta}$	$\frac{\xi_4}{\zeta}$
A1	18.8	1	0.18(1)	1	-	-	-
A2	28.8	0.0095	0.83(7)	0.47(2)	-0.53(2)	-	-
A3	18.8	0.0034	2.6(4)	0.21(2)	-0.45(1)	0.34(2)	-
A4	31.7	$7.3 \times 10^{-6}$	44(6)	0.03(1)	-0.16(1)	0.46(1)	-0.35(1)

i.e., the ratio of the heaviest resonance's contribution to the LSRs to the total resonance contribution to the sum-rules. Using values of  $m_i$  and  $\xi_i$  from Tables III and V respectively, this ratio evaluates to 0.43. In the axial vector channel, an analogous ratio measuring the relative contribution to the LSRs of  $m_4$  gives 0.25.

Employing QCD LSRs, we studied conventional meson-hybrid meson mixing in vector and axial vector charmonium-like channels. Using measured masses as inputs, we tested experimentally observed resonances for coupling to both conventional and hybrid meson currents, i.e., for meson-hybrid mixing. In both channels, agreement between QCD and hadron physics was significantly improved by the inclusion of resonances above 4 GeV. In the vector channel, we found that conventional meson-hybrid meson mixing was well-described by a two resonance scenario consisting of the  $J/\psi$  and a 4.3 GeV state. These results are consistent with the  $J/\psi$  being predominantly a conventional meson but with a small hybrid meson compo-

nent. As for the heavier state, it has been speculated that the  $Y(4260)$  has a significant hybrid meson component (see [8], for example), an interpretation consistent with our findings. In the axial vector channel, we found almost no mixing in the ground state,  $\chi_{c1}(1P)$ , minimal mixing in the  $X(3872)$ , and significant mixing in both the  $X(4140)$  and  $X(4274)$ . Ref. [9] argues that the  $X(3872)$  has a significant conventional meson component while Ref. [10] argues that it has a significant hybrid meson component. Our results are compatible with either conclusion, but have difficulty accommodating both.

#### Acknowledgments

We are grateful for financial support from the National Sciences and Engineering Research Council of Canada.

- 
- |  |   |
|--|---|
| <p>[1] N. Brambilla <i>et al.</i>, Eur. Phys. J. <b>C71</b> (2011) 1534, 1010.5827.</p> <p>[2] Particle Data Group, C. Patrignani <i>et al.</i>, Chin. Phys. <b>C40</b> (2019) 100001.</p> <p>[3] M. A. Shifman, A. I. Vainshtein, and V. I. Zakharov, Nucl. Phys. <b>B147</b> (1979) 385.</p> <p>[4] M. A. Shifman, A. I. Vainshtein, and V. I. Zakharov, Nucl. Phys. <b>B147</b> (1979) 448.</p> <p>[5] A. Palameta, J. Ho, D. Harnett, and T. G. Steele, Phys. Rev. <b>D97</b> (2018) 034001, 1707.00063.</p> | <p>[6] A. Palameta, D. Harnett, and T. G. Steele, Phys. Rev. <b>D98</b> (2018) 074014, 1805.04230.</p> <p>[7] D. Binosi <i>et al.</i>, Compute. Phys. Commun. <b>180</b> (2009) 1709, 0811.4113.</p> <p>[8] S.-L. Zhu, Phys. Lett. <b>B631</b> (2005) 212, hep-ph/0507025.</p> <p>[9] R. D. Matheus <i>et al.</i>, Phys. Rev. <b>D80</b> (2009) 056002, 0907.2683.</p> <p>[10] W. Chen <i>et al.</i>, Phys. Rev. <b>D88</b> (2013) 045027, 1305.0244.</p> |
|--|---|